RSC Advances

PAPER

Check for updates

Cite this: *RSC Adv.*, 2023, **13**, 11525

Highly stable Fe/CeO_2 catalyst for the reverse water gas shift reaction in the presence of H_2S†

Ryo Watanabe, *[a] Fumiya Karasawa,[a] Chikamasa Yokoyama,[a] Kazumasa Oshima,[b] Masahiro Kishida,[b] Masahiro Hori,[c] Yukinori Ono,[c] Shigeo Satokawa,[d] Priyanka Verma [a] and Choji Fukuhara*[a]

Received 27th February 2023
Accepted 29th March 2023

DOI: 10.1039/d3ra01323e

rsc.li/rsc-advances

This study focused on evaluating the catalytic properties for the reverse water gas shift reaction (RWGS: $CO_2 + H_2 \rightarrow CO + H_2O$ $\Delta H^0 = 42.1$ kJ mol^{-1}) in the presence of hydrogen sulfide (H_2S) over a Fe/CeO_2 catalyst, commercial Cu–Zn catalyst for the WGS reaction (MDC-7), and Co–Mo catalyst for hydrocarbon desulfurization. The Fe/CeO_2 catalyst exhibited a relatively high catalytic activity to RWGS, compared to the commercial MDC-7 and Co–Mo catalysts. In addition, the Fe/CeO_2 catalyst showed stable performance in the RWGS environment that contained high concentrations of H_2S. The role of co-feeding H_2S was investigated over the Fe/CeO_2 catalyst by the temperature programmed reaction (TPR) of CO_2 and H_2 in the presence of H_2S. The result of TPR indicated that the co-feeding H_2S might enhance RWGS performance due to H_2S acting as the hydrogen source to reduce CO_2.

1. Introduction

Most of the world's natural gas resources are in the form of sour gas, which contains high concentrations of hydrogen sulfide (H_2S) and carbon dioxide (CO_2), with typical compositions of 0–30 vol% H_2S and 0–80 vol% CO_2.[1–3] Sour gas is widely distributed worldwide, including in the Middle East, Canada, Northern Europe, and China. High concentrations of H_2S (over 30 vol%) is contained in large gas fields in Saudi Arabia, Abu Dhabi, and offshore areas in Iran.[4] Moreover, biogas, a renewable energy source that has attracted much attention in recent years, contains a relatively high concentration of H_2S.[5–7] In order to use the hydrocarbons in natural gas or methane in biogas as fuel, pollutants (H_2S and CO_2) that exist beyond allowable limits must be removed. For example, in natural gas, the heavy hydrocarbons are condensed and then passed through a scrubbing unit typically composed of liquid amine-based adsorbents to remove the sour gas components (H_2S and CO_2), in a process called "sweetening".[8] However, the liquid amine sorbents cannot control the H_2S/CO_2 selectivity because the concentration of these contaminants varies depending on the source of the natural gas.[9,10] In this regard, acid gas remediation is costly, and it is often uneconomical to extract and use natural gas resources that contain high concentrations of acid gases. In many cases, most of the recovered CO_2 and H_2S is buried in landfills.[11,12] This has necessitated the exploration of new strategies for the active use of C and S-containing substances (CO_2 and H_2S) to address the critical issues of global climate change and sustainability. H_2S, one of the sour gas components, is known to cause catalytic deactivation; hence, its academic value and economic benefits are expected to be significant if S-resistant catalysts can be used to directly convert the CO_2 in sour natural gas into value-added products.

There has been extensive research on high-performance catalysts for CO_2 conversion in the presence of H_2S. Sharma *et al.* reported that MoS_2 was effective for CO_2 hydrogenation under relatively high concentrations (<2500 ppm) of H_2S.[13] They suggested that H_2S acts as a "conduit" for the active hydrogen required for the hydrogenation of CO_2, contributing to the enhancement of activity. Guilera *et al.* investigated the S resistance of Ni/Al_2O_3 doped with rare-earth oxides of CeO_2 and La_2O_3 for the low-temperature hydrogenation of CO_2.[14,15] They reported that even in an atmosphere containing low concentrations (0.4 ppm) of H_2S, the Ni-based catalysts were not deactivated by sintering or S poisoning. To the best of our knowledge, there have only been a few reports on S-resistant CO_2 conversion catalysts. Our group studied the dehydrogenation of alkanes in the presence of high concentrations of H_2S (several tens of vol%), and found that Fe-based catalysts showed high activity and high selectivity with a stable performance.[16,17]

[a]Department of Applied Chemistry and Biochemical Engineering, Graduate School of Engineering, Shizuoka University, 3-5-1 Johoku, Naka-ku, Hamamatsu, Shizuoka 432-8561, Japan. E-mail: watanabe.ryo@shizuoka.ac.jp; fukuhara.choji@shizuoka.ac.jp

[b]Department of Chemical Engineering, Faculty of Engineering, Kyushu University, 744 Motooka Nishi-ku, Fukuoka-shi, Fukuoka 819-0395, Japan

[c]Research Institute of Electronics, Shizuoka University, 3-5-1 Johoku, Naka-ku, Hamamatsu, Shizuoka 432-8561, Japan

[d]Department of Materials and Life Science, Faculty of Science and Technology, Seikei University, 3-3-1 Kichijoji Kitamachi, Musashino-shi, 180-8633, Tokyo, Japan

† Electronic supplementary information (ESI) available. See DOI: https://doi.org/10.1039/d3ra01323e

Therefore, we focused on Fe as a component as it is effective in water gas shift (WGS) reactions, and CeO_2 as the support because of its excellent functionality for CO_2 conversion.[18–22] By employing an Fe-supported CeO_2 (Fe/CeO_2) catalyst in the reverse water gas shift (RWGS) reaction, a highly stable performance is expected even when the reaction atmosphere contains a high concentration of H_2S. In this study, the characteristics of the RWGS reaction using the Fe/CeO_2 catalyst with/without H_2S co-feeding were compared with those of the reaction using a commercial Cu–ZnO catalyst (MDC-7) and Co–Mo-based desulfurization catalyst, which are known to exhibit catalytic performance even in a high concentration of H_2S in the atmosphere. In addition, the stability of the Fe/CeO_2 catalyst was investigated over a reaction time of 12 h while co-feeding H_2S. The structure of the catalyst after the reaction was qualitatively investigated by X-ray diffraction (XRD) and STEM-EDX mapping to estimate the structure of the Fe and Ce component phases in the RWGS atmosphere in the presence of H_2S. Furthermore, to identify the effect of H_2S on the RWGS, the reaction mechanism was estimated by the temperature programmed reaction (TPR) with CO_2 and H_2 in the presence of H_2S.

2. Experimental

2.1. Preparation and characterization of the catalyst

The Fe/CeO_2 catalyst was prepared by an impregnation method. The CeO_2 (JRC-CEO-2) catalyst support was provided by the Catalysis Society of Japan. First, 2.0 g of CeO_2 was immersed in 30 mL of distilled water for 6 h, following which 1.624 g of $Fe(NO_3)_3 \cdot 9H_2O$ was added and stirred for an additional 2 h. The Fe-based catalyst was then calcined at 500 °C for 1 h. The loading amount of Fe was 10 wt%. MDC-7 (Clariant Catalysts K.K.), with 34 wt% Cu, was used for comparison with the Fe/CeO_2 catalyst. The reference Co–Mo-based catalyst was prepared by a previously reported method.[23] Some promoters of Zn and P components were included in the reference Co–Mo-based catalyst. The crystal structures of the Fe species and Ce species in the Fe/CeO_2 catalyst were determined *via* XRD (Ultima IV, Rigaku) using a Cu Kα radiation source. The elemental mapping of the Fe/CeO_2 catalyst after the RWGS with H_2S co-feeding was performed by STEM-EDX (JEM-2100F, JEOL, Japan). The element maps of the Fe, Ce, S, and O components of the Fe/CeO_2 catalyst were collected for investigating the dispersion of the Fe components and coverage of the S atoms on the catalyst.

2.2. Evaluation of catalytic performance

Catalytic reaction tests were conducted at ambient pressure in a fixed bed reactor. After placing the catalyst in the center of the reaction tube, H_2 reduction (100 vol%) was carried out at 500 °C for 1 h. After purging the reduction gas, the reaction temperature was set at 400 to 600 °C, the catalyst amount was 75 mg, and the reaction gas with the composition $CO_2/H_2/H_2S/He$ was supplied at $40/40/x/20 - x$ mL min^{-1} ($x = 0$–10). The gas was quantified by an FID gas chromatograph (GC-2014, Shimadzu, Japan) and FPD gas chromatograph (GC-2030, Shimadzu, Japan).

2.3. Temperature programmed reaction method

To clarify the reaction mechanism of the RWGS, TPR analysis was carried out with the following steps. First, the Fe/CeO_2 catalyst of 100 mg was pretreated with the gas composition of $H_2/Ar = 25/5$ mL min^{-1} at 500 °C. After 1 h of the pretreatment, the reduced gas was purged by He, following the catalyst temperature was decreased to 40 °C. Then, CO_2 with co-feeding H_2S (gas composition: $CO_2/H_2S/Ar/He = 1/1/5/93$ mL min^{-1}) was supplied to the catalyst with increasing temperature from 40 °C to 800 °C. After that, the catalyst temperature was decreased to 40 °C, again. Subsequently, H_2 with co-feeding H_2S (gas composition: $H_2/H_2S/Ar/He = 1/1/5/93$ mL min^{-1}) was supplied with increasing temperature from 40 °C to 800 °C. The produced gases in these operations were monitored by a quadrupole mass spectrometer (QMS, HIDEN ANALYTICAL, UK).

3. Results and discussion

3.1. Effect of H_2S on RWGS performance

The performance of the Fe/CeO_2 catalyst was evaluated and compared with those of the reference MDC-7 and Co–Mo catalysts. The Co–Mo catalyst has been reported to be highly active in WGS reactions involving H_2S. Hence, this catalyst was used as a desulfurization catalyst, and its RWGS performance was evaluated. Fig. 1 shows the effect of the H_2S concentration on the CO_2 conversion of the Fe/CeO_2, and commercial MDC-7 and Co–Mo catalysts at various reaction temperatures. The RWGS reaction selectively proceeded since the selectivity to CO was *ca.* 100% under all conditions. For the Fe/CeO_2 catalyst, the CO_2 conversion increased with increasing reaction temperature, and reached 29.6% at 600 °C. Compared to its RWGS performance with no H_2S, there was no significant decrease in the catalytic performance at H_2S concentrations of 1, 5 and 10%. In other words, the performance of the Fe/CeO_2 catalyst was not adversely affected by H_2S. There has been no report on the catalyst for RWGS almost not degrading under a high

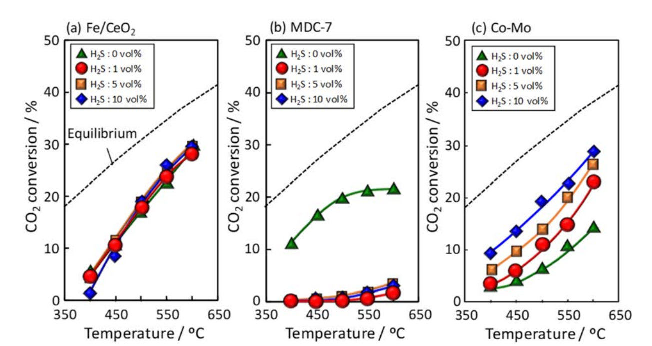

Fig. 1 Effect of H_2S co-feeding on the RWGS performance of (a) Fe/CeO_2, (b) MDC-7, and (c) Co–Mo catalysts. The reaction conditions were as follows: the catalyst amount was 75 mg, gas composition was $CO_2/H_2/H_2S/He = 40/40/x/20 - x$ mL min^{-1} ($x = 0$–10), and reaction temp. ranged from 400 to 600 °C. Note that sel. of CO was 100%.

concentration of H_2S. The performance of the MDC-7 catalyst was superior to that of the Fe/CeO_2 catalyst. However, there was no significant increase in activity with increasing temperature, which is possibly attributed to the sintering and oxidation of the active Cu component by the water vapor produced during the progress of the RWGS reaction.[24] In addition, the co-feeding of H_2S greatly decreased the RWGS activity on the MDC-7 catalyst, where the CO_2 conversion was approximately 1.7% at 600 °C under 1 vol% H_2S. Interestingly, the degradation of the Cu-based catalyst progressed with the coexistence of H_2S, while that of the Fe/CeO_2 catalyst was almost negligible. For the Co–Mo catalyst, in a H_2S-free atmosphere, the WGS performance was low, but with increasing H_2S concentration, improved. In particular, the highest WGS performance was observed under 10 vol% H_2S. Although the Co–Mo catalyst was effective under a high concentration of H_2S, the Fe/CeO_2 catalyst showed better performance under a low concentration of H_2S, which indicated that the Fe/CeO_2 catalyst could be applicable to the biogas.

To evaluate the durability of the Fe/CeO_2 and Co–Mo catalysts, long-term RWGS reaction was tested under 1 vol% of H_2S. Moreover, to determine the role of the Fe component and CeO_2 support, RWGS tests were carried out over the Fe/SiO_2 and bare CeO_2 catalysts. Fig. 2 shows the CO_2 conversion over the Fe/CeO_2 and Co–Mo catalysts with the reaction time. When H_2S was supplied, the CO_2 conversion was high for 12 h over the Fe/CeO_2 catalyst. Since the products mostly contained CO, the RWGS selectively proceeded over the Fe/CeO_2 catalyst. Compared with the RWGS performance of the Co–Mo catalyst, that of the Fe/CeO_2 catalyst was superior, with high stability. The Fe/SiO_2 and bare CeO_2 catalysts were less active than the Fe/CeO_2 catalysts, indicating that both, Fe and CeO_2, are required for the RWGS when co-feeding H_2S. Since CeO_2 had a low activity and Fe/SiO_2 exhibited almost no activity, it was assumed that there might be an interaction between the Fe and CeO_2 components.

3.2. Structure characterization

To investigate the structure of the Fe/CeO_2 catalyst, XRD and STEM-EDX analyses were performed on the catalysts after the RWGS with H_2S co-feeding (Fig. 3(a) and (b), respectively). From Fig. 3(a), regardless of the change in the H_2S concentration, no

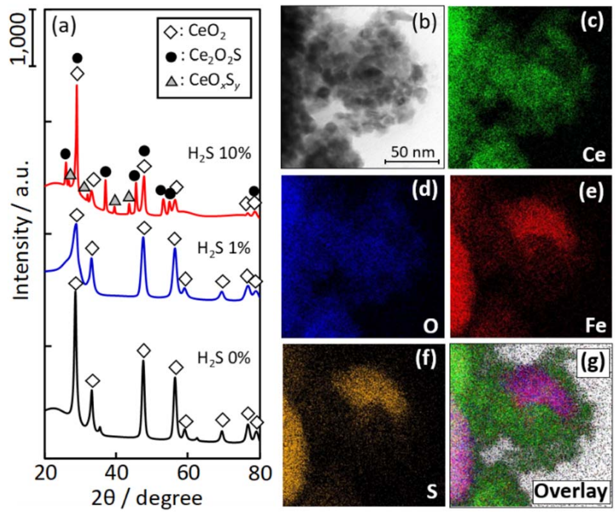

Fig. 3 (a) XRD pattern and (b)–(g) STEM-EDX mapping of the Fe/CeO_2 catalyst after RWGS with H_2S co-feeding.

diffraction peaks of the Fe component are observed and only the Ce component is detected. Further, only CeO_2 is detected when the H_2S concentrations are 0 vol% and 1 vol%, and the peak intensity of CeO_2 decreases with increasing H_2S supply. When the H_2S concentration is further increased from 1 vol% to 10 vol%, the CeO_2 phase transforms into oxysulfates of Ce_2O_2S and $Ce_2O_xS_y$. From the atomic mapping of Fig. 3(b), the Fe species are dispersed on the CeO_2 support; however, there are some areas where the Fe species are heavily segregated. The Fe mapping is visually similar to the S mapping, which suggests the absorption of S species on the Fe species in the catalyst. ESI 1† shows the thermodynamically stable phases of the Fe component from 25 °C to 700 °C in the reaction simulated gas atmosphere of CO and H_2, and H_2S. Since $Fe_{0.877}S$ (major phase) and FeS (minor phase) are the stable phases of Fe species at the reaction temperature from 25 °C to 700 °C, the S identified from the STEM-EDX mapping is assumed to be incorporated in a sulfide phase.

Fig. 4 shows the Raman spectra of the Fe/CeO_2 catalyst after RWGS with different hydrogen sulfide concentrations (1 vol% and 10 vol%). Some peaks attributed to pyrrhotite (FeS_x) were observed at 213 cm^{-1}, 277 cm^{-1}, and 391 cm^{-1} for the Fe/CeO_2 catalyst after RWGS containing 1 vol% and 10 vol% of H_2S.[26] The results are roughly in agreement with those inferred from thermodynamic calculations, as shown in ESI 1.†

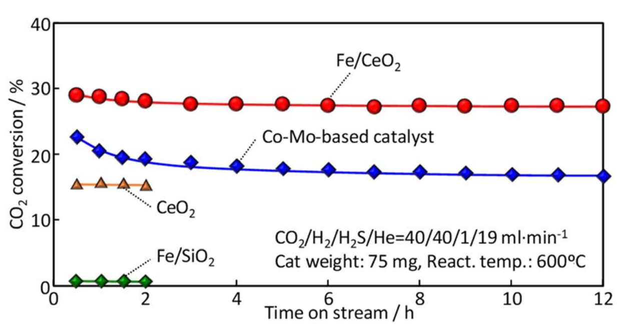

Fig. 2 Performances of Fe/CeO_2, Co–Mo, Fe/SiO_2, and CeO_2 catalysts for the RWGS with 1 vol% H_2S at 600 °C. Note that sel. of CO was 100%.

3.3. Role of H_2S

To clarify the role of H_2S in the Fe/CeO_2 catalyst on the RWGS reaction, a TPR analyses were performed. Fig. 5(a) and (b) respectively show the profile of product during the CO_2-TPR and H_2-TPR analyses. The products were detected by a quadrupole mass spectrometer, where the temperature was increased by 10 °C min^{-1}, along with supplying 1 vol%-CO_2 or 1 vol%-H_2 in the presence of 1 vol%-H_2S to the Fe/CeO_2 catalyst. The shaded area indicated the amount change of each gas; positive area

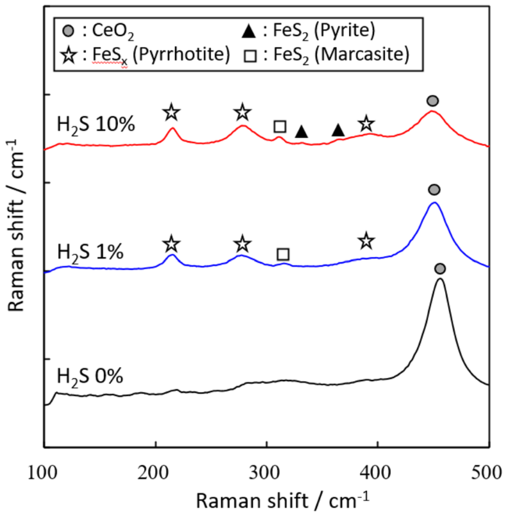

Fig. 4 Raman spectra of the Fe/CeO_2 after RWGS with H_2S co-feeding.

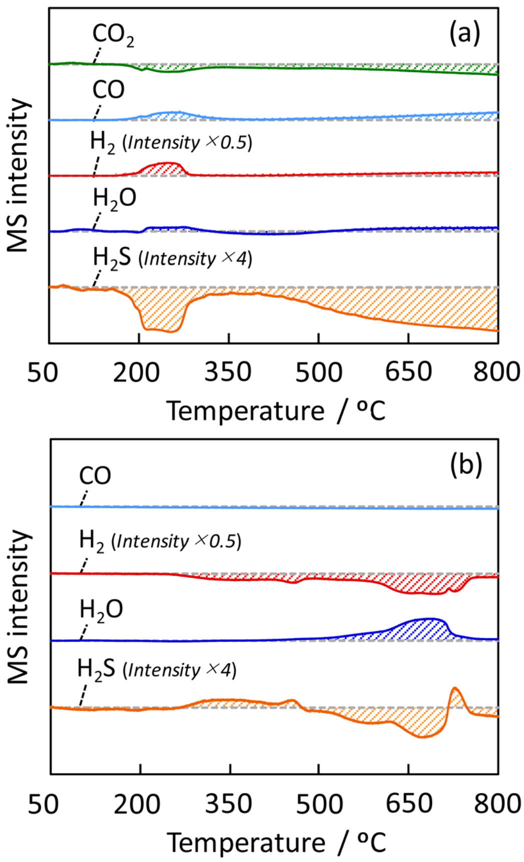

Fig. 5 Products behavior in TPR with (a) CO_2 and (b) H_2 in the presence of H_2S over the Fe/CeO_2 catalyst. The H_2 and H_2S intensities were adjusted because the sensitivity was quite different from the other products.

represents generation, and negative area represents consumption. By flowing CO_2 to the Fe/CeO_2 catalyst, CO is observed to form at from 180 °C to 350 °C. At the same temperature of the formation of CO, the production of H_2 and H_2O and the consumption of H_2S were observed. The above phenomena can be understood as follows; H_2 generated by sulfurization of the Fe/CeO_2 catalyst is thought to have reduced CO_2 to form CO. Similarly, at temperatures above 350 °C, H_2S was consumed to generate H_2, and CO_2 was reduced to CO. The reason for the consumption of H_2S and CO_2 in both low (180–350 °C) and high temperature (T > 350 °C) regions is thought to be due to the formation of the lattice sulfide ion (S^{2-}) by feeding H_2S on both the surface and the bulk of the catalyst. As confirmed by Fig. 5(b), H_2 was consumed at around 250 °C by the reaction with lattice S^{2-} ($H_2 + S^{2-} \rightarrow H_2S + V_S$). In this experiment, H_2-TPR is performed after CO_2-TPR; the regeneration of lattice S^{2-} from H_2S during CO_2-TPR was considered to contribute the formation of H_2S at low temperature from 250 to 400 °C. Furthermore, the formation of H_2O can be observed at temperatures above 500 °C. The result meant that a lattice oxygen was generated by catalyst oxidation ($CO_2 + V_{ox} \rightarrow CO + O^{2-}$) in CO_2-TPR, and followed by the consumption of generated lattice oxygen by H_2 to produce H_2O.

Fig. 6 exhibits the ESR signal of oxygen and/or sulfur vacancy after TPR with CO_2 and H_2. The vacancy was confirmed at g = 2.03 before the reaction, due formation of lattice vacancy in CeO_2.[25] After TPR with CO_2 and H_2 with H_2S, the peak at g = 2.03 was not also confirmed, indicating that the vacancy was replenished as S^{2-}/O^{2-} by H_2S/CO_2. Based on these data, H_2S might act as a sulfidizing-agent in the Fe/CeO_2 catalyst, meaning that generated lattice vacancy was replenished rapidly by S^{2-}. To confirm this assumption, H_2S was supplied to the Fe/CeO_2 catalyst before the reaction. It is clear from this figure that the peak at g = 2.03 originating from defects has almost disappeared. The result suggests that the following reaction ($H_2S + V \rightarrow S^{2-} + H_2$) proceeds and restores lattice S^{2-} to the vacancy.

The role of H_2S was discussed from the viewpoint of reaction mechanism. The reaction pathway envisioned is that CO_2 is activated on the surface of the CeO_2 support[27] and reduced to CO by reacting with hydrogen activated by FeS_x. The coexisting H_2S is also expected to regenerate lattice S^{2-} to produce activated H atoms, and this generated hydrogen species further activates CO_2. In other words, the generated H_2 from H_2S on the

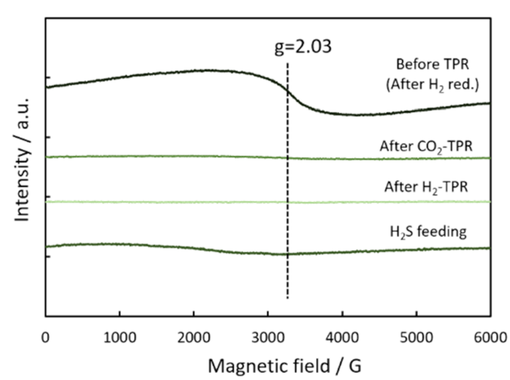

Fig. 6 ESR signal of the Fe/CeO_2 catalyst before TPR (after H_2 reduction), after H_2S feeding, after CO_2-TPR and H_2-RPR.

catalyst could work as hydrogen source to CO_2 reduction. In the case of Fe/CeO_2, the activity does not change much when the gas-phase H_2S concentration is changed because the bulk diffusion of lattice S^{2-} is the rate-limiting factor. In the Co–Mo system, on the other hand, the performance is greatly enhanced by the H_2S concentration, so we expect that $H_2S \rightarrow H_2$ (active H species) $+S^{2-}$ at the catalyst surface is the rate-limiting factor.

4. Conclusions

The catalytic properties of Fe/CeO_2 and MDC-7 catalysts for the RWGS reaction with H_2S co-feeding were evaluated. MDC-7 showed a relatively high activity in the low-temperature range, but underwent significant deactivation during the RWGS with H_2S co-feeding. The Fe/CeO_2 catalyst similarly showed a relatively high activity for the RWGS, and showed a stable activity for 12 h in the reaction atmosphere containing H_2S. The result TPR with CO_2 and H_2 indicated that co-feeding H_2S might act as the hydrogen source for RWGS over the Fe/CeO_2 catalyst.

Conflicts of interest

There are no conflicts to declare.

Acknowledgements

This work was supported by the Uncharted Territory Challenge 2050, New Energy and Industrial Technology Development Organization (NEDO), Japan.

References

1 W. F. J. Burgers, P. S. Northrop, H. S. Kheshgi and J. A. Valencia, *Energy Procedia*, 2011, **4**, 2178–2184.
2 W. Taifan and J. Baltrusaitis, *Catal. Sci. Technol.*, 2017, **7**, 2919–2929.
3 N. W. Chakroun and A. F. Ghoniem, *Int. J. Greenhouse Gas Control*, 2015, **41**, 163–173.
4 A. Hofmann, W. van Strien, and R. Malekzadeh, in, *Abu Dhabi International Petroleum Exhibition & Conference*, OnePetro, 2017.
5 Y. Belmabkhout, G. De Weireld and A. Sayari, *Langmuir*, 2009, **25**(23), 13275–13278.
6 J. I. Huertas, N. Giraldo and S. Izquierdo, *Mass transfer in chemical engineering processes*, 2011.
7 P. Iovane, F. Nanna, Y. Ding, B. Bikson and A. Molino, *Fuel*, 2014, **135**, 352–358.
8 W. Y. Lee, S. Y. Park, K. B. Lee and S. C. Nam, *Energy Fuels*, 2020, **34**(2), 1992–2000.
9 K. Huang, X. M. Zhang, X. B. Hu and Y. T. Wu, *AIChE J.*, 2016, **62**, 4480–4490.
10 K. Huang, D. N. Cai, Y. L. Chen, Y. T. Wu, X. B. Hu and Z. B. Zhang, *ChemPlusChem*, 2014, **79**(2), 241–249.
11 C. Khan, R. Amin and G. Madden, *J. Pet. Explor. Prod. Technol.*, 2013, **3**, 55–60.
12 A. Y. Kaita, O. Ogolo, X. Wu, I. Mohammed and E. A. Akpan, *J. Pet. Explor. Prod. Technol.*, 2020, **10**, 1575–1589.
13 L. Sharma, R. Upadhyay, S. Rangarajan and J. Baltrusaitis, *ACS Catal.*, 2019, **9**, 10044–10059.
14 J. Guilera, J. D. Valle, A. Alarcón, J. A. Díaz and T. Andreu, *J. CO_2 Util.*, 2019, **30**, 11–17.
15 A. Alarcón, J. Guilera, R. Soto and T. Andreu, *Appl. Catal., B*, 2020, **263**, 118346.
16 R. Watanabe, N. Hirata, Y. Yoda, Y. Fushimi and C. Fukuhara, *J. Jpn. Pet. Inst.*, 2020, **63**(4), 228–237.
17 R. Watanabe, N. Hirata, K. Miura, Y. Yoda, Y. Fushimi and C. Fukuhara, *Appl. Catal., A*, 2019, **587**, 117238.
18 Y. Sekine, T. Chihara, R. Watanabe, Y. Sakamoto, M. Matsukata and E. Kikuchi, *Catal. Lett.*, 2010, **140**(3), 184–188.
19 R. Watanabe, Y. Sakamoto, K. Yamamuro, S. Tamura, E. Kikuchi and Y. Sekine, *Appl. Catal., A*, 2013, **457**, 1–11.
20 C. Fukuhara, K. Hayakawa, Y. Suzuki, W. Kawasaki and R. Watanabe, *Appl. Catal., A*, 2017, **532**, 12–18.
21 S. Ratchahat, M. Sudoh, Y. Suzuki, W. Kawasaki, R. Watanabe and C. Fukuhara, *J. CO_2 Util.*, 2018, **24**, 210–219.
22 C. Fukuhara, A. Kamiyama, M. Itoh, N. Hirata, S. Ratchahat, M. Sudoh and R. Watanabe, *Chem. Eng. Sci.*, 2020, **219**, 115589.
23 N. Nakajima, Y. Seriguchi, M. Kato, M. Yoshinari, T. Yoshida and K. Watanabe, *J. Jpn. Pet. Inst.*, 2013, **56**(6), 388–394.
24 C.-S. Chen, W.-H. Chen and S.-S. Lin, *Appl. Catal., A*, 2004, **257**, 97–106.
25 X. Chen, S. Zhan, D. Chen, C. Hea, S. Tian and Y. Xiong, *Appl. Catal., B*, 2021, **286**(5), 119928.
26 Y. El Mendili, A. Abdelouas, H. El Hajja and J.-F. Bardeau, *RSC Adv.*, 2013, **3**, 26343.
27 F. Cao, Y. Xiao, Z. Zhang, J. Li, Z. Xia, X. Hu, Y. Ma and Y. Qu, *J. Catal.*, 2022, **414**, 25–32.

